Title
ATOMIC SCATTERING FROM A SINUSOIDAL HARDWALL: COMPARISON OF APPROXIMATE METHODS WITH EXACT QUANTUM RESULTS

Author
Masel, Richard I.

Publication Date
1976-04-01

Submitted to Journal of Chemical Physics

LBL-4969
Preprint c.1

ATOMIC SCATTERING FROM A SINUSOIDAL HARDWALL: COMPARISON OF APPROXIMATE METHODS WITH EXACT QUANTUM RESULTS

Richard I. Masel, Robert P. Merrill, and William H. Miller

April 1976

Prepared for the U. S. Energy Research and Development Administration under Contract W-7405-ENG-48

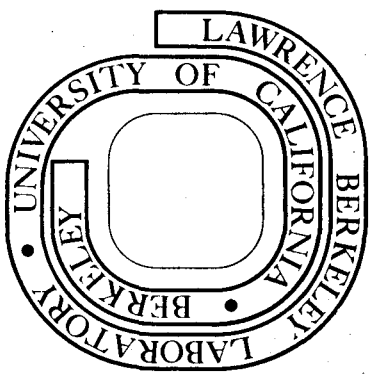

DISCLAIMER

LBL-4969

ATOMIC SCATTERING FROM A SINUSOIDAL HARDWALL: COMPARISON OF APPROXIMATE METHODS WITH EXACT QUANTUM RESULTS

by

Richard I. Masel, Robert P. Merrill

Department of Chemical Engineering

University of California

Berkeley, California 94720

and

William H. Miller

Department of Chemistry, and Materials and Molecular

Research Division of the Lawrence Berkeley Laboratory,

University of California, Berkeley CA 94720

April, 1976

Abstract

Several approximate procedures for the calculation of the intensities of atoms elastically scattered from solids are compared with nearly exact quantum calculations from a sinusoidal hardwall potential. The quasiclassical method reproduces the qualitative features of the "rainbow" envelope of the scattered intensities present in the exact results but it does not contain any of the quantum interference arising from multiple scattering within a single unit cell and thus does not reproduce the rich structure in the intensities of individual diffraction beams. CCGM theory predicts only specular scattering for the hardwall, independent of roughness. Semiclassical theory at normal incidence gives the same analytical result as the Kirchoff approximation. This result agrees to within 3% of the exact calculations for surface roughness from 0.02 to 0.1 of a lattice constant, a, at ka vectors greater than 22. At lower ka vectors deviations as large as 60% are observed for the 0.1 roughness while at 0.02 roughness deviations are still less than 2%. Renormalization of the results from the 0.1 surface reduces its deviations from the exact calculation to less than 10% even at low ka vectors. The Kirchoff result agrees with the semiclassical only at normal incidence and can be used only for hardwall potentials.

1. Introduction

In recent years, many theories have been advanced, which attempt to explain the results of diffractive atom surface scattering experiments [1]. In an attempt to do the calculations exactly, Wolken [2] and Tsuchida [3] numerically integrate coupled channelled equations, a procedure that is, in principle, exact (with an infinite number of channels), but requires extensive computation. Beeby [4] uses a Greens function technique, which, for a surface of hard spheres, reduces to a KKR-like procedure. This method is weakly convergent, and in addition, the scattering boundary conditions used have been questioned [5].

Approximate methods include the Kirchoff (or Eikinol) approximation of Levi et al. [6] and Berry [7], the CCGM method of Goodman et al. [8], the semiclassical approximation of Doll [9] and Masel et al. [10], and the quasiclassical method of Bowman [11].

CCGM [8] is essentially a unitarized first order Born method. One starts with a weak coupling formalism, and uses an a priori unitarization procedure to extend it to a strong coupling limit. The procedure can, in principle, be used for any interaction potential and inelastic effects can be included fairly simply. The major disadvantage is that its range of validity is largely unknown, so that the quantitative success of the theory has not been demonstrated. Still, the procedure has been used extensively, and many (but not all) of the results obtained are at least qualitatively reasonable.

The Kirchoff approximation used by Levi [6] and Berry [7] is an adaptation of a well-established approximation from acoustics and optics [12]. It is a useful approximation, for surfaces that are not too rough, with near normal angles of incidence. It often gives analytical expressions for the scattering distribution. It is, however, limited to surfaces that can be approximated as a hard wall. This is a severe limitation and as will be discussed later leads to unphysical surface morphologies when the surface potential is relatively soft.

The semiclassical approximation used by Doll [9] and Masel et al. [10] is an extension of the methods used by Miller [14] and Marcus [15] for scattering of atoms and molecules in the gas phase. The approximation is useful when the momentum of the incident particles is large and there is not too much classical multiple scattering. It has not yet been extensively tested for surface scattering, but it has been shown to be in semi-quantitative agreement with experimental data [10].

The quasiclassical method is similar to the semiclassical method, except that phase interferences are ignored, and the intensities are averaged over a range of scattered angles assigned to each diffracted beam. Bowman [11] claims that this procedure is in excellent agreement with the coupled channel calculations of Wolken, but such agreement is not obvious from the calculations presented.

This paper is an attempt to assess the utility of the approximate methods (CCGM, Kirchoff, semiclassical, and quasi-classical) for the case of atom surface scattering by comparing them to the exact solution [13] for scattering at normal incidence

from a sinusoidal hard wall at moderate roughnesses. The results show that the CCGM procedure gives qualitatively incorrect results for this example, while the Kirchoff and semiclassical approximations are in essential quantitative agreement with the exact results, except at low energies. The low energy semiclassical results can be brought into agreement with the exact results with the use of an ad hoc renormalization procedure. Comparison of hard and soft wall calculations shows that the major effect of the hard wall assumption is to accentuate the surface roughness. Surface morphologies deduced from experimental data via the hard wall theories would therefore be much smoother than the actual surface. It should be noted here that Doll [9] has shown that the semiclassical calculations are in reasonable agreement with the soft wall calculations of Wolken [2], although extensive comparison was impractical due to the numerical complexity of Wolken's procedure. Doll's results along with the results presented here suggest that the semiclassical theory is useful over a wide range of interactions while the CCGM and Kirchoff approximations seem to fail in either the hard or soft wall limit.

The quasi-classical approach is devoid of any interference phenomena except that artificially imposed to designate which of the classical trajectories contribute to each "diffraction beam". As a result it does produce qualitatively the basic "rainbow structure" of the exact solution, but fails to yield any Bragg-maxima in the intensity as a function of energy.

2. The Exact Solution

In an earlier paper [13], we presented a rigorous calculation of the scattering pattern from a sinusoidal hard wall. The derivation is based on the Lippmann-Schwinger equation:

$$\psi(r) = \Phi_I(r) + \int dr' G_o^+(r,r') V(r') \psi(r') \tag{1}$$

where

$\psi(r)$ is the wavefunction

$\Phi_I(r)$ is the incident wave

$G_o^+(r,r')$ is the outward-going free particle Green's function and

$V(r)$ is the potential.

If the potential is of the form

$$V = 0 \qquad z \geq D(x) \tag{2}$$

$$V = \infty \qquad z < D(x)$$

where

z = distance above the surface

x = distance along the surface

$D(x)$ = the surface contour

then it can be shown

$$V(r)\psi(r) = f(x)\delta(Z-D(x)) \tag{3}$$

where $f(x)$ is a function of x yet to be determined.

Combining equations 1 and 3 yields

$$\psi(x,z) = \Phi_I(x,z) + \int dx'\, dz'\, G_o^+(x,z,x',z') f(x') \delta[z' - D(x')] \tag{4}$$

An incident plane wave

$$\Phi_I(r) \equiv e^{ik(\sin\theta_I x - z\cos\theta_I)} \tag{5}$$

and a sinusoidal surface

$$D(x) \equiv ha \cos\frac{2\pi x}{a} \tag{6}$$

are assumed. Expanding f(x) in a Fourier series:

$$f(x) = \sum_n e^{i(k\sin\theta_I + \frac{2\pi n}{a})x} \tag{7}$$

and solving for the condition that $\psi(r) = 0$ below the surface yields, for $z \geq ha$

$$\psi(r) = \Phi_I(r) + \sum_\ell S_\ell \Phi_\ell(r) \tag{8}$$

where $\Phi_\ell(r)$ is the eigenfunction corresponding to the ℓ th order diffraction beam and

$$S_\ell \equiv \sum_{n=-\infty}^{\infty} C_n J_{\ell-n}(hka\cos\theta_\ell) \tag{9}$$

The coefficients C_n are determined by the infinite matrix equation

$$\cos\theta_I \delta_{\ell,o} = \sum_n C_n J_{n-\ell}(hka\cos\theta_\ell) \tag{10}$$

This is a banded matrix and only the C_n that satisfy $|n| \leq N$ were considered in equations 7 and 8. N was increased until numerical convergence was obtained. While this is not, in principle, an exact procedure, by suitable choice of N, the error can be made arbitrarily small, and so, for comparison purposes, the procedure can be considered to be exact.

Some of the results of the calculations are shown in fig. 1. At low incident k vectors, the scattering patterns show a strong specular peak and only weak diffraction features. At higher incident k vectors, a rainbow pattern begins to appear. If the surface roughness, h, is increased, the diffraction features and the rainbow patterns will appear at a lower energy, and the rainbow angles will be further apart. Qualitatively, this is the behavior observed in rare gas scattering from metallic and alkali halide surfaces [1].

For the purpose of comparison, we will focus on h = 0.02 (a relatively smooth surface) and h = 0.10 (a relatively rough one). In the flat surface (h = 0) limit, all of the approximate methods converge to the correct result (only specular scattering), and so a comparison in the nearly flat surface region is not instructive. It should also be noted that all of the comparisons are for normal incidence, and that intensities in this paper are defined so that they satisfy the normalization condition

$$\sum_{\ell} I_{\ell} \frac{\cos\theta_I}{\cos\theta_{\ell}} = 1 \qquad (11)$$

where the sum goes over all ℓ, satisfying

$$\ell \leq \frac{ka}{2\pi}$$

2.1. A reformulation of the exact calculations.

The exact formulation presented in the last section, while very useful for numerical calculations, suffers from the defect that it reveals very little of the physics of the scattering process. When f(x) is expanded in a Fourier series much of the physics is obscured. In this section we will reformulate the scattering problem so that the physics is more transparent. The reformulation will be used primarily for qualitative comparisons, though it could, in principle, be used for quantitative calculations also.

The Lippmann-Schwinger equation, equation 1, provides the basis for an iterative solution of the scattering problem. Starting with an initial trial wave function $\psi_o(r)$, a new approximation $\psi_1(r)$ can be calculated using

$$\psi_n(r) = \Phi_I(r) + \int dr' G_o^+(r,r') V(r') \psi(r')_{n-1} \tag{12}$$

where n is the order of the approximation.

If such a procedure converges, then it will produce the exact result, but it will only converge through a very judicious choice of ψ_o. If any ψ_n has a non-zero part below the surface, the integral becomes infinite, and so the procedure will never converge. Notice though that the true wave function is zero everywhere on and below the surface. Defining a heavy-sided function, q(Z) in the standard manner

$$q(z) = \int_{-\infty}^{z} \delta(0) dz \tag{13}$$

with δ, the dirac delta function. For any function $\Gamma(x,z)$ the relation

$$\psi(x,z) = q(z-D(x)) \left[\psi(x,z) + \Gamma(x,z) \right] \tag{14}$$

will hold exactly provided $\Gamma(x,z) = 0$ on and above the surface.

Define a function $\widehat{\psi}(x,z)$ by

$$\widehat{\psi}(x,z) = \psi(x,z) + \Gamma(x,z) \tag{15}$$

where $\Gamma(x,z)$ is a special function chosen so that $\widehat{\psi}$ and all

of its derivatives are continuous in the region $z \geq D(x) - \Delta$ and $\Delta \rightarrow 0^+$. There are an infinite number of Γ that satisfy this condition, one is

$$\Gamma(x,z) = -\psi(x',z') \tag{16}$$

with

$$x' = p(x,z) - x \tag{17}$$

$$z' = g(x,z) + 2D(x) - z$$

and $p(x,z)$ and $g(x,z)$ are a solution of

$$0 = \frac{\partial\psi(x,z)}{\partial x}\bigg|_{z=D(x)+\Delta} \frac{\partial p(x,z)}{\partial x} + \frac{\partial\psi(x,z)}{\partial x}\bigg|_{z=D(x)+\Delta} \left(\frac{\partial g(x,z)}{\partial x} + 2\frac{dD(x)}{dx}\right) \tag{18}$$

$$0 = \frac{\partial\psi(x,z)}{\partial dx}\bigg|_{z=D(x)+\Delta} \frac{\partial p(x,z)}{\partial z} + \frac{\partial\psi(x,z)}{\partial z}\bigg|_{z=D(x)+\Delta} \frac{\partial g(x,z)}{\partial z}$$

with the boundary condition:

$$p(x,D(x)) = g(x,D(x)) = 0$$

Starting with the Schroedinger equation

$$\left[\frac{\hbar^2}{2m}\left(\frac{\partial^2}{\partial x^2} + \frac{\partial^2}{\partial z^2}\right) + E\right]\psi = V\psi \tag{19}$$

Substituting 12 and 13 into the left hand side yields

$$\frac{\hbar^2}{2m}\left[\hat{\psi}(x,z)\left(\frac{\partial^2 q}{\partial z^2} + \frac{\partial^2 q}{\partial x^2}\right) + 2\left(\frac{\partial q}{\partial x}\frac{\partial\hat{\psi}}{\partial x} + \frac{\partial q}{\partial z}\frac{\partial\hat{\psi}}{\partial z}\right)\right] + q\frac{\partial^2\psi}{\partial x^2} + \frac{\partial^2\psi}{\partial z^2} + E\hat{\psi} = V\hat{\psi} \tag{20}$$

The arguments in our previous paper [13] show that $V\psi$ is zero everywhere but on the surface. For $z = D(x)$, $\psi(x)$ is identically zero, and since all of the derivatives of ψ are continuous,

$$V\psi = \frac{\hbar^2}{m}\delta(z-D(x))\left[\frac{\partial D(x)}{\partial x}\frac{\partial\hat{\psi}}{\partial x} + \frac{\partial\hat{\psi}}{\partial z}\right] \tag{21}$$

f(x) in equation 3 becomes

$$f(x) = \frac{\hbar^2}{m}\left(\frac{\partial D(x)}{\partial x}\frac{\partial \hat{\psi}}{\partial x} + \frac{\partial \hat{\psi}}{\partial z}\right) \tag{22}$$

Defining the unit surface normal η and arc length s in the usual way

$$\underset{\sim}{\eta} = \frac{1}{\left(\frac{\partial x}{\partial s}\right)}\left(\frac{\partial D(x)}{\partial x}\underset{\sim}{u}_x + \underset{\sim}{u}_z\right) \tag{23}$$

$$\frac{\partial s}{\partial x} = \sqrt{1 + \left|\frac{\partial D(x)}{\partial x}\right|^2}$$

where $\underset{\sim}{u}_x$ and $\underset{\sim}{u}_z$ are unit vectors in the x and z directions.

Combining equations 22 and 23 yields

$$f(x) = \left(\left.\frac{\partial \hat{\psi}}{\partial \underset{\sim}{\eta}}\right|_{z = D(x)}\frac{\partial s}{\partial x}\right)\left(\frac{\hbar^2}{2m}\right) \tag{24}$$

and since all of the derivatives of ψ are continuous, and

$\psi = 0$ for $z \geq D(x)$

$$f(x) = \left[\left(\left.\frac{\partial \psi}{\partial \underset{\sim}{\eta}}\right|_{z = D(x) + \Delta}\right)\left(\frac{\partial s}{\partial x}\right)\right]\left(\frac{\hbar^2}{2m}\right)$$

which gives a physical interpretation to f(x).

Combining equations 4 and 24

$$\psi_n(r) = \Phi_I(r) + \int dr\, G_o^+(r;r')\left[\delta(z-D(x))\left.\frac{\partial \psi n-1}{\partial \eta}\right|_{\substack{x=x' \\ z=D(x')+\Delta}}\frac{\partial s}{\partial x}\right. \tag{25}$$

$$= \Phi_I(r) + \frac{\hbar^2}{2m}\int dx' G_o^+(x,z;\, x',z' = D(x'))\left.\frac{\partial \psi}{\partial \eta}\right|_{\substack{x=x' \\ z=D(x')+\Delta}}\left.\frac{\partial s}{\partial x}\right|_{x=x'} \tag{26}$$

This result can also be derived from the Hemholtz equation which can be written

$$\psi(r) = \frac{\hbar^2}{2m}\int_C ds\left(G_o\frac{\partial \psi}{\partial \eta} + \psi\frac{\partial G_o}{\partial \eta}\right) \tag{27}$$

where $\int G_o = \left(\frac{\hbar v^2}{2m} + E\right)^{-1}$, and $\int_C$ indicates an integral over any contour in free space, and $\psi(r)$ is the wave function in free space.

For the contour $z = D(x) + \Delta$, when $\Delta \to 0^+$, ψ is zero by continuity and since the surface only generates outward-going waves this becomes

$$\psi = \Phi_I + \int G_o^+ \, dS \, \frac{\partial \psi}{\partial \underset{\sim}{n}} \quad z = D(x) + \Delta \tag{28}$$

which is essentially the same as equation 26. A direct derivation of equation 28 from the Lippmann-Schwinger equation is given in Appendix D. We note that equation 28 has been used by DeSanto (16), with the boundary condition $\psi = 0$ on the surface to derive a system of equations equivalent to equations 8-10.

Equation 26 is a prescription for an interative calculation of the scattered wave: starting with an initial guess, $\psi_o = \Phi_I$ the incident wave, and solving iteratively for ψ_1, ψ_2, ... yields (assuming convergence) better and better approximations to the wave function. A physical interpretation of the procedure may be helpful. In going from ψ_o to ψ_1, the wave function was forced to zero under the surface (via equation 12). The scattered waves that are produced during this process are calculated via equation 10. In essence then, in going from ψ_o to ψ_1, the wave function undergoes a single reflection, and so the name "single scattering approximation" for ψ_1 seems appropriate. In going from ψ_1 to ψ_2, etc., the waves may be thought to scatter successively (multiple scattering) until convergence. For future reference, this type of multiple scattering will be labelled "quantum multiple scattering". It occurs even when the surface is flat, and thus the flat surface warrants some further discussion.

Assuming ψ_o, the incident wave, is given by

$$\psi_o = \Phi_I = e^{i(k_x x - k_z z)} \tag{29}$$

direct application of equation 21 for D(x) = 0 yields,

$$\psi_1 = e^{i(k_x x - k_z z)} - \frac{1}{2} e^{i(k_x x + k_z |z|)} \tag{30}$$

$$\psi_2 = e^{i(k_x x - k_z z)} - \frac{3}{4} e^{i(k_x x + k_z |z|} \tag{31}$$

and in general

$$\psi_n = e^{i(k_x x - k_z z)} - (1 - (\tfrac{1}{2})^n) e^{i(k_x x + k_z |z|)} \tag{32}$$

In the $n \to \infty$ limit, the correct result (13) is obtained.

$$\psi = e^{i(k_x x - k_z z)} - e^{i(k_x x + k_z |z|)} \tag{33}$$

This procedure can be rationalized by viewing the surface as a series of points separated by a differential distance. When the incident wave hits one of these points, it acts as though it were an isolated pole in the potential and emits the spherically symmetric outward-going wave. Since the wave is spherically symmetrical, half of the flux scatters away from the surface and half of the flux propagates into the surface.

There are many points on the surface, and so a large portion of the spherical wave is destroyed through phase cancellation, i.e., these channels are closed. The only thing that survives is the part of the spherical wave that satisfies $\Delta k_x = 0$, the only open channel for a flat surface[†].

[†]This follows directly from the diffraction condition. The flat surface can be considered to be a periodic surface with lattice dimension a. The Laue condition implies that the relation $\frac{\Delta K_x}{2\pi} = j/a$ j is an integer must be satisfied for all choices of a. The only way that this condition can be satisfied is for j = 0, which implies $\Delta k_x = 0$.

The wave function is then an inward-going plane wave, and two scattered waves, one of which propagates away from the surface in the specular direction, and one of which propagates into the surface in the incident direction, partially cancelling the incident wave. The two scattered waves have the same intensity. Therefore in the single scattering approximation,

$$\psi = \psi_1 = e^{i(k_x x - k_z z)} - \frac{1}{2}\left(q(z)e^{i(k_x x + k_z z)} + q(-z)e^{i(k_x x + k_z z)}\right) \quad (34)$$

The minus sign comes in because of the reflection.
One can verify that this is the same ψ_1 as in equation 30.

For a hard wall, there cannot be any penetration of the wave into the surface, and so the wave multiply scatters. Again it produces a spherical wave with half of the flux going out of the surface and half of the flux moving into the surface. After phase cancellation, the resultant wave function is ψ_2.

In the rough surface case, there is an additional form of "quantum multiple scattering" which occurs because the spherical wave hits the surface at a point separate from the incident wave. This form of multiple scattering is also excluded from ψ_1 since ψ_o has been taken to be the incident wave. It is not excluded from ψ_2 because ψ_1, the "incident wave" for double scattering, contains strong non-specular components. For the purpose of this discussion, it will not be necessary to distinguish between these two forms of quantum multiple scattering.

2.2. CCGM calculations

Goodman and his coworkers [8] use a unitarized first order distorted wave Born procedure, called CCGM, to interpret atom surface scattering data. Starting with the Schroedinger equation, equation 19, the wave function is first expanded in terms of the

eigenfunctions of the potential averaged in the x and y (in-plane) directions. The wave function can then be expressed as a Born series, which is summed by assuming that the principle (i.e., real) part of the Greens function is negligible, except in the single quantum scattering limit.

After many manipulations, the result is a simple matrix equation which relates the amplitude of the various peaks, D_G, to the matrix elements of the Fourier transform of the potential, $A_{\alpha\beta}^{GG'}$.

$$i\lambda_\alpha^G D_g = -A_{\alpha 0}^G(1-\delta_{G,0}) + i\sum_{G'\neq G}\sum_\beta A_{\alpha\beta}^{GG'} D_G^\beta \tag{35}$$

with

λ_α^G = a dimensionless energy defined in equation 3.13 of ref. 8a

$A_{\alpha\beta}^{GG'}$ = (constant) $(\alpha|V_{G-G'}|\beta)$

where

$$V_G = \frac{1}{L^2}\int_{-L/2}^{L/2} \partial y \int_{-L/2}^{L/2} dx\, V(x,y,z)e^{iG\cdot r}$$

and α and β are various eigenstates of V_o.

The intensities of the various peaks, R_F, can be calculated from

$$R_F = \left|\delta_{F,0} - 2iD_F^F\right|^2 \tag{36}$$

If none of the diffracted peaks are related by a reciprocal lattice vector [8], then

$$R_{F\neq 0} = 4\left|\frac{A_{F0}}{\Delta}\right|^2 \tag{37}$$

$$R_0 = 1 - \sum_{F\neq 0} R_F$$

$$\Delta = 1 + \sum_{F\neq 0}\left|A^{F0}\right|^2 + i\sum_{G\neq 0}\sum_m \frac{A_{m0}^{G0}}{\lambda_m^G}^2$$

In order to calculate the A matrix elements, it is necessary to redefine the potential in 2. For algebraic simplicity, the following potential was assumed.

$$V = 0 \qquad Z > ha\cos\left(\frac{2\pi x}{a}\right)$$

$$V = \frac{w\pi}{\cos^{-1}(z/B)} \qquad -B \leq z \leq ha\cos\left(\frac{2\pi x}{z}\right) \tag{38}$$

$$V = W \qquad z \leq -ha$$

where eventually the limit as $w \to \infty$ will be taken.

Admittedly this potential is unusual, but it is continuous everywhere but on the boundary, and it does approach the potential given by equation 2 in the limit that $w \to \infty$. In the derivation of equations 4 and 5, it was not necessary to know how the potential approached infinity, and so they should apply to the potential given by 38 as well as the potential in 2. Further it is not at all unreasonable to have poles in an otherwise finite potential (e.g., at the positions of the ion cores).

The potential averaged in the y and z directions is

$$V_o = 0 \qquad z > ha \tag{39}$$

$$V_o = W \qquad z \leq ha$$

Its eigenvalues can be found by inspection.

$$\Phi_{k_z} = \sqrt{\frac{2}{c_{k_z}}}\, e^{ik_z \cdot z} \qquad z \geq ha$$

$$= \sqrt{\frac{2}{c_{k_z}}}\, \exp\sqrt{\frac{2mw}{\hbar^2} - k_z^2}\,(z - ha) + ik_z ha \qquad z \leq ha$$

where the constants c_{k_z} are determined by a box normalization condition.

$$\delta_{k_z^1, k_z^2} = \int_{-L/2}^{L/2} \Phi_{k_z^1}\, \Phi_{k_z^2}\, dz \tag{40}$$

one should verify that for $w > \frac{\hbar^2 k^2}{2m}$

$$c_{k_z} = L \qquad \text{for } k_z \text{ real}$$

$$c_{k_z} = \left| e^{ik_z B}\left[\frac{1}{\sqrt{\frac{2mw}{h^2} - k_z^2} + ik_z} - \frac{1}{ik_z}\right]\right| \tag{41}$$

In order to calculate the A matrix elements, terms of the form

$$(K_{F_z}|V_H|K_{G_z})$$

must be calculated. In Appendix A, it is shown

$$(K_{F_z}|V_H|K_{G_z}) = \frac{2\delta_{H_y,0}\, ha\, we^{-\xi}\, Be^{i[G_z - F_z^*]\, ha}}{\sqrt{c_k c_F}} \tag{42}$$

with

$$\xi = ha\left(\sqrt{\frac{2mw}{\hbar^2} - G_z^2} + \sqrt{\frac{2mw}{\hbar^2} - F_z^2}\right) \qquad j = \frac{Hxa}{2\pi} \tag{43}$$

and

$$B = \int_0^{\pi} dU\, \frac{\sin U \sin jU}{jU}\, e \cos U \tag{44}$$

which can be evaluated as

$$B = \sum_{n=0}^{\infty} b_n\, \sigma(j,n) \tag{45}$$

with $b_n = 2\, I_n(\xi)$

$$b_o = I_o(\xi) \tag{46}$$

and

$$\sigma[j,n] = \int_0^{\pi} dU\, \frac{\sin U \sin jU \cos nU}{jU} \tag{47}$$

for $j \neq 0$, this is

$$\sigma[j,n] = \frac{1}{4j}\Big[\mathrm{Cin}(|n + j + 1|\pi) + \mathrm{Cin}(|j + 1 - n|\pi) - \mathrm{Cin}(|n - j - 1|\pi) - \mathrm{Cin}(|n + j - 1|\pi)\Big]$$

One is referred to p. 244 in Abramowitz [17] for a definition and numerical table of the Cin function.

Using Abromowitz [18] 9.7.1, one can easily show that for large w

$$(K_{F_z}|V_H|K_{G_z}) = \left\{ \frac{\delta_{H_y,0} e^{i(G_z - F_z^*)B}}{\sqrt{c_k c_F}} \sqrt{\frac{B}{\pi\sqrt{\frac{2m}{\hbar^2}}}} \right\}$$

$$\left\{ \left[\sigma[j,0] + 2\sum_n \sigma[j,n]\right] w^{3/4} + \right.$$

$$\left. \left[\frac{1}{8\sqrt{\frac{2M}{\hbar^2}}}\right]\left[\sigma[j,0] + 2\sum_n \sigma[j,N]\left[4n^2 - 1\right]\right] w^{1/4} + O(w^{-1/4}) \right\} \qquad (48)$$

More details are given in Appendix A.

In the limit $w \to \infty$, all of the A matrix elements will approach infinity (or zero, it does not matter which). From equation 39, one can show that all of the D matrix elements approach zero, so that only specular scattering is allowed*, independent of h. A very unphysical result.

---

*This result is more obvious from equation 37, although strictly speaking equation 37 is not applicable to this case.

In retrospect this result is not surprising. With an infinite hard wall, the average potential, $V_o(z)$ is infinite for $z < ha$. The eigenfunctions of V_o are therefore zero for $z \leq ha$ and so they do not sample the potential, except at $z = ha$. At this point the hard wall is flat, and so only specular scattering is predicted. Of course the real wave function is not zero for $z > ha \cos\frac{2\pi x}{a}$, and so there is also non-specular scattering.

This effect is not limited to the hard wall. Whenever there are strong variations of the potential in the x and y directions, the wave function will also vary rapidly in these directions. CCGM uses a wave function based on the average potential, which cannot reproduce these variations. Effectively, CCGM smooths out the potential, which leads to a more specular scattering pattern. It is interesting to note, that unless some adjustment factor is used (e.g., surface steps), the CCGM procedure seems to predict greater specular scattering than is normally observed. Goodman [8] suggests that this is because of problems with the experimental data. We suggest that it may be that the CCGM basis set is not appropriate whenever the variations in the potential in the x and y directions are large.

This, however, is not the only problem with CCGM in the strong interaction limit. In the derivation of equation 35, it was necessary to ignore the principle part of the Greens function. In the case of a hard wall, the principle part of the Greens function is infinite, so it is difficult to see how it could be ignored. Rabitz [18] has shown that for atom-diatom

scattering, a unitarized Born procedure, using appropriate wave functions does not give physically meaningful results in the strong interaction limit. For an interaction of intermediate strength, it does give qualitatively useful results. Unitarized Born, if done correctly, is slightly better than a simple Born procedure, but it should not be expected to produce quantitative results except where the potential is weak.

2.3. The semiclassical approximation

Another approximation that has been successful is the semiclassical approximation used by Doll et al. [9] and Masel et al. [10]. It is based on a similar approximation developed for gas phase scattering by Miller [14] and Marcus [15]. To understand the approximation physically, one must recall the discussion of the multiple scattering process in section 2.1. When the incident wave hits the surface, scattered waves originate from every point on the surface, and propagate in every direction. In order to obtain discrete beams, most of the waves must interfere destructively. When these interferences are included, only those beams that satisfy the diffraction condition are allowed. Each point on the surface can be thought of as generating a series of beams in the allowed directions. Closer examination however reveals that due to additional interference, each point on the surface does not radiate equally; some of the beams are stronger than others, and some points on the surface produce a strong contribution to the scattering profile while other points contribute weakly.

One can show that those points on the surface that lie on a classical path through phase space connecting the incident beam to a diffracted state have the largest effect on the scattering profile. In the semiclassical approximation only those points that lie on the classical path are included. One can show that this will be a good approximation whenever the classical action of the path is large compared to $\hbar$, which means it will be best at high energies and with massive particles (in atomic units). It should be valid for all potentials, but since it is a generalization of the WKB approximation it should work best when the potential is soft. The hard wall, then, is a good test of the semiclassical approximation, because if the approximation is successful here, it should work on most real potentials.

In the semiclassical approximation the amplitude of a given beam, S_ℓ is calculated as a sum of amplitudes S_ρ of the various classical paths ρ connecting the incident wave to a diffracted state*.

$$S_\ell = \sum_\rho S_\rho \tag{49}$$

---

*Note that the normalization condition on the S_ℓ is

$$\sum_{|\ell| \leq \frac{ka}{2}} |S_\ell|^2 = 1$$

In order to use this equation, one must first find the classical paths. More precisely, given a classical particle with a momentum equal to the momentum of the incident wave, one must find the scattered angle as a function of the initial position. It is convenient to represent this information in the form of a classical deflection function; i.e., a plot of the final direction of the particle as a function of $\hat{x}$, the projection of its initial position onto the xy-plane.

For a two-dimensional system

$$\hat{x} \equiv \lim_{z\to\infty} \; x - z \frac{k_x^o}{k_z^o} \tag{50}$$

where k_x^o and k_z^o are the initial x and z components of the particles's momentum.

The deflection function can be calculated in a number of ways. The most exact way is to integrate numerically the classical trajectories. This, however, does not yield an analytic expression for the deflection function (and therefore the scattering profile). An analytic expression for the scattering profile can be obtained, however, if the incident particle only undergoes one classical reflection from the surface during the scattering process. This approximation, which we shall use here, is not inherent in the theory and is only necessary because an analytic expression is desired. In Appendix C, the validity of the approximation is examined.

Generally, it is valid if the scattering angle θ obeys

$$|\theta| \leq |\arccos(2h)| \tag{51}$$

and the surface roughness h satisfies

$$h \leq h^*(\theta_I) = c_1 \frac{(1 - |\sin\theta_I|)}{\cos\theta_I} \tag{52}$$

where c_1 is a constant between .130 and .143.

We note that the single classical scattering approximation is a much less severe approximation than the assumption of single scattering in the quantum sense, i.e., $\psi = \psi_1$ (see equation 30), and is exact for a flat surface.

In the single classical scattering limit, the scattered angle can be calculated in terms of the x component of the point where the trajectory hits the surface x*, as follows

$$\theta(x^*) = 2 \tan^{-1}\left[2\pi h \sin\left(\frac{2\pi x^*}{a}\right)\right] + \theta_I \tag{53}$$

$\hat{x}$ is related to x* by

$$\hat{x} = x^* - \frac{k_x^o}{k_z^o} D(x^*) \tag{54}$$

For normal incidence, equation 54 may easily be inverted analytically, and we will restrict our discussion to that case.

At normal incidence,

$$\hat{x} = x^* \tag{55}$$

which fixes the deflection function.

Once the deflection function is known, it is a simple matter to calculate the intensities, following the procedures outlined in our previous paper [10]. Appendix B shows that the uniformized intensity, P_ℓ, of the ℓth diffraction peak is given by

$$P_\ell = \left\{ J_\ell \left[kha \left(1 + \sqrt{1 - \frac{2\pi\ell}{k_a}} \right)^2 \right] \right\}^2 \tag{56}$$

where the intensities are normalized as in equation 11 and J_ℓ is the ℓth order Bessel function.

It should be noted that equation 56 is in qualitative agreement with our exact calculations. A quantitative comparison will follow after a discussion of the Kirchoff approximation, which gives similar results to the semiclassical approximation for hard wall scattering.

2.4. The Kirchoff approximation

Levi et al. [6] and Berry [7] use a very standard approxmiation from acoustics and optics called the "Kirchoff Approximation". It essentially assumes that the potential is hardwall-like, and that the semiclassical approximation applies. In addition, it assumes that (1) there is no classical multiple scattering (i.e., the deflection function in equation 53 is valid independent of the h and θ_I and (2) the condition

$$\widehat{x} = x^* \tag{57}$$

holds at all incidence angles

When these approximations are made, an analytical expression for the scattering intensities can easily be derived using the same methods used to derive equation 56. The result is

$$P_\ell = J_\ell^2 \left[kha(\cos\theta_I + \cos\theta_\ell) \right] \tag{58}$$

which is identical to equation 56 at normal incidence. It may be shown, however, that there is a systematic difference between the phase of the scattered wave given by Levi's derivation of the Kirchoff approximation and that given by the complete semiclassical theory.

Levi, et al. [6] have derived equation 58 in a somewhat different manner. They start with the Rayleigh equation and then make a single scattering (in the quantum sense) approximation, to get a diagonal matrix. Semiclassical methods are used to evaluate the matrix elements to give equation 58 for the intensities. Superficially, one would expect these assumptions to limit the Kirchoff approximation to high energies and small values of h, but we shall see that the final result, equation 58, works very well (better than the Rayleigh solution). The reason is due to a gross cancellation of errors. The Rayleigh equation itself is not the unique solution of the scattering problem [5] and is, in fact, divergent when $h > .0714$ [19]. The single scattering approximation to the Rayleigh equation is a better result in that it is no longer divergent and, in fact, is analytically identical to the true quantum single scattering limit, except for phase. The semiclassical methods used to evaluate the matrix elements restores most of the quantum multiple scattering. The final result, equation 58, works very well, then, provided: (1) the single classical scattering limit applies; (2) shadowing is unimportant; and (3) the hardwall potential applies.

Both assumptions (1) and (2), above, hold fairly well when the conditions in equations 51 and 52 are satisfied for all of the prominent beams (with θ_I replaced by θ_ℓ, the scattering angle). But assumption (3) is not generally valid. Doll has derived an analytical expression, which can be used to estimate the surface roughness, provided the potential can be approximated by a hard wall [9]. Good agreement is obtained for helium scattering from a stiff potential such as that of He/LiF. However, when this equation is applied to a softer potential such as He/W<112>,

the predicted surface roughness is about a factor of 3 too small. There is a major difference between the two potentials. It is best seen by looking at a comparison of the classical trajectories for He scattering from a hard (stiff) and soft potential shown schematically in fig. 2.

In the case of a stiff potential, the trajectory hits the repulsive wall and turns around very quickly, so it only samples a small portion of the potential. In the case of the soft potential, the trajectory penetrates deeply and samples much of the unit cell, which has the effect of averaging the potential over a large portion of the unit cell. Of course, the averaged potential is much smoother than the real potential[†]. When the potential is assumed to be hard wall-like, this averaging process is ignored. If a hardwall theory is used to deduce the amplitude of the surface periodicity from scattering data from a soft potential, it leads to a prediction of amplitudes which are too small, and therefore to an unreal surface morphology. The Kirchoff approximation assumes a hardwall potential, and so can predict unphysical surface morphologies. The semiclassical method is not limited to hardwall potentials.

2.5. Comparison of the quantum results to the semiclassical and Kirchoff approximations

In figs. 3-5, the semiclassical approximation to the scattering intensity, of the specular, first and second order diffracted beams, at normal incidence, with h = 0.02 is compared to the exact quantum results. The agreement between the two sets of curves is very good. The average difference between the two curves is less than 2%. This is certainly within the accuracy of any published scattering experiment.

[†]This is one reason why metal surfaces have always appeared to be much smoother than alkali-halide surfaces.

Even so, there are some discernable differences between the two sets of curves. The most obvious difference is that the semiclassical curve is shifted slightly with respect to the quantum curve. While we have no physical explanation of this shift, it is most easily seen when the surface roughness is small, and is not noticeable when hka $\geq$ 1.3. Of course, when hka is small, the stationary phase approximation is the poorest and so it is not entirely surprising that the semiclassical approximation is not exact in this region.

One should note that at low energies, the semiclassical approxmiation does not satisfy the normalization condition equation 11, while the quantum result satisfies it (to within .0001) everywhere. This is a problem that was noted in our previous paper [10]. To correct it, all of the intensities in the previous paper were renormalized via an ad hoc procedure

$$I_\ell^R = \frac{I_\ell}{\sum_{\ell \quad |\ell| \leq \frac{ka}{2\pi}} I_\ell \frac{\cos\,\theta_I}{\cos\,\theta_\ell}} \tag{59}$$

where I_ℓ^R equals the renormalized intensities.

Renormalized curves are also presented in figs. 3-5. At roughnesses this low, renormalization makes little difference in the intensity profile. It does, however, correct some errors when k is small.

Fig. 6 is a plot of the intensity of the specular beam as a function of the k vector for a much rougher surface (h = 0.10). For ka greater than 21, the simple semiclassical theory works very well, but at k-vectors less than 20, deviations start to

become significant. Fortunately, most of the errors are corrected by renormalization, but there still are some residual errors for ka between 17 and 21. This is a very unusual region in the figure. Semiclassically, the first Bragg maximum in the specular peak occurs at ka = 19.2. The second order diffraction feature moves through the rainbow angles at ka = 19.1. The competition between these two events, we believe, causes the cusp in the curve. In the simple semiclassical theory, the competition between the two events is ignored entirely, so the cusp is not reproduced.

2.6. Quasiclassical calculations

Bowman [11] has suggested that the intensity of the various diffraction beams can be obtained by assuming that the incident beam behaves classically, and calculating the fraction of trajectories that scatter to within 1/2 a diffraction order of each diffraction maxima. For the hard wall surface, then,

$$I_n = \frac{\sum_{\rho} \int_{-b_J(n-1/2)}^{b_J(n+1/2)} db}{a} \qquad (60)$$

where

I_n = the intensity of the nth order beam

$b_J(\ell)$ = the impact parameter that leads to scattering at diffraction order ℓ

ρ = an index that allows for the fact that there may be more than one classical trajectory that scatters in any direction.

For a hard wall surface, for h < .13, the single scattering detection function derived in the appendix applies.

Putting this in equation 60 and noting that there are two classical trajectories that scatter at any angle yields:

$$I_n = -\frac{1}{\pi}\left\{\arcsin\left[\frac{ka}{(2n+1)\pi}\,\frac{1}{2\pi h}\left(1-\sqrt{1-\left(\frac{(2n+1)\pi}{ka}\right)^2}\right)\right] - \arcsin\left[\frac{ka}{(2n-1)\pi}\,\frac{1}{2\pi h}\left(1-\sqrt{1-\left(\frac{(2n-1)\pi}{ka}\right)^2}\right)\right]\right\}$$

where the argument of the arc sin is assumed to be no greater than 1 in absolute value.

A plot of this function for n = 0 and h = .10 function of ka is shown in fig. 7 for conditions identical to figure 6. It is monotonically decreasing and does not reproduce the bragg-like intensity profile seen in the semiclassical and quantum calculations

Though Bowman [11] claims reasonable agreement with Wolken's results [2] it is obvious that none of the quantum interference structure is present in the quasiclassical method, and it is not at all clear how the simplistic averaging of the deflection function over a finite momentum window associated with each diffraction channel could approach the accuracy of the semiclassical calculations. It certainly does not for hard wall scattering.

3. Conclusion

In this paper, various approximate theories for atom-surface scattering were compared to the quantum results for scattering off a sinusoidal hard wall. When applied to an infinite step potential, the CCGM model predicts only specular scattering, independent of roughness. This unphysical result occurs because the CCGM approximation assumes that the wavefunction can be expanded in terms of the eigenfunctions of the average potential. In the hard wall case, it is obvious that this assumption is incorrect. In addition, CCGM assumes that the principle part of the Greens function is negligible. This assumption is not valid in the hard wall case where the principle part can be infinite.

In general CCGM can only be applied quantitatively to a "weak coupling" system. In surface scattering, it is not obvious what constitutes "weak coupling". One should note that with $h \to 0^+$, all of the diffraction peaks will be very small, and yet this does not constitute "weak coupling" in the sense of the CCGM approximation.

The quasiclassical approximation has the correct qualitative rainbow structure but lacks any vestige of quantum interference which results from multiple scattering within a single unit cell and does not predict the correct intensities.

In contrast to these rather poor approximations, the Kirchoff and semiclassical approximations give near quantitative results for scattering from a sinusoidal hard wall, except at low k-vectors. These errors are corrected partially by renormalization.

The Kirchoff approximation, however, is only usable when the potential can be approximated by a hard wall and only classical single scattering trajectories contribute to the major scattering intensities. The semiclassical approximation is not limited to these situations, though difficulties arise here also for strong multiple scattering in the classical trajectories. Nevertheless the semiclassical approximation seems to be by far the most generally applicable approximate formalism of those in current use.

4. Acknowledgements

This work has been supported by the U. S. Energy Research and Development Administration, by AFOSR Grant No. 76-2926 and NSF Grant No. GP-39317. One of us (W.H.M.) acknowledges support from a Camille and Henry Dreyfus Teacher-Scholar Grant. We also thank F. Goodman for comments on the CCGM hardwall calculations.

TABLE I

INCIDENCE ANGLE	CRITICAL H CALCULATED NUMERICALLY	CRITICAL H CALCULATED VIA EQU C5 WITH HO=.13	CRITICAL H CALCULATED VIA EQU C5 WITH HO=.143
0.	.130000	.130000	.143000
.100	.119427	.117609	.129370
.200	.109292	.106292	.116921
.300	.099660	.095864	.105450
.400	.090440	.086178	.094796
.500	.081586	.077115	.084826
.600	.073057	.068574	.075431
.700	.064812	.060472	.066519
.800	.056813	.052739	.058013
.900	.049024	.045314	.049845
1.000	.041397	.038143	.041957
1.100	.033935	.031180	.034298
1.200	.026595	.024382	.026820
1.300	.019350	.017710	.019481
1.400	.012173	.011129	.012242
1.500	.005039	.004604	.005064

APPENDIX A

Calculation of $(K_{F_z}|V_H|K_{G_z})$

In the CCGM procedure, it is necessary to calculate matrix elements of the Fourier components of the potential. This appendix outlines the details of this calculation.

Starting with the potential defined previously

$$V = 0 \qquad z > ha\cos(2\pi x/a)$$

$$V = \frac{w}{\cos^{-1}(z/ha)} \qquad -ha \leq z \leq ha\cos\frac{2\pi x}{a}$$

$$V = w \qquad z \leq -ha$$

where eventually $w \to \infty$.

One can verify that V_o, the average potential, is given by

$$V_o = 0 \qquad z > ha$$

$$V_o = w \qquad z \leq ha$$

The eigenfunctions of V_o, Φ_{k_z} can be calculated by inspection, for $w > \frac{\hbar^2 k^2}{2m}$

$$\Phi_{k_z} = \sqrt{2/c_{k_z}}\; e^{ik_z \cdot z} \qquad z \geq ha$$

$$= \sqrt{2/c_{k_z}}\; \exp\left[\sqrt{\frac{2mw}{\hbar^2} - k_z^2}\,(z - ha) + ik_z ha\right] \qquad z \leq ha$$

where

$$c_{k_z} = L \qquad \text{for } k_z \text{ real}$$

$$c_{k_z} = \left| e^{ik_z ha}\left[\sqrt{\frac{2mw}{\hbar^2} - k_z^2} + k_z - \frac{1}{ik_z}\right]\right| \qquad \text{for } k_z = i|k_z|$$

The Fourier components of the potential V_H are also easily found

$$V_H = \frac{1}{L^2}\int_{\text{surface}} V(r)e^{iH\cdot t}d^2r$$

$$= \delta_{H_y,0}\int_{-1/2}^{1/2} d(x/a)\; V(\tfrac{x}{a},z)\; e^{iH_x a(\frac{x}{a})}$$

$$= w\delta_{H,0} \qquad z \leq -ha$$

$$= 0 \qquad z > ha$$

$$= \frac{2\pi\delta_{H_y,0}w\,\sin\left[\frac{aH_x}{2\pi}\cos^{-1}(z/ha)\right]}{H_x a\cos^{-1}(z/ha)} \qquad |z| \leq ha$$

It is necessary to calculate matrix elements like

$$(K_{F_z}|V_H|K_{G_z})$$

letting $j = \frac{H_x a}{2\pi}$

$$(K_{F_z}|V_H|K_{G_z}) = \frac{2ha\delta_{H_y,0}we^{i\left(G_z - F_z^*\right)ha}}{j\sqrt{c_G c_F}}\int_{-1}^{1} d(z/ha)\,\frac{\sin[j\cos^{-1}(z/ha)]}{\cos^{-1}(a/ha)}\,e^{i[(z/ha)-1]Q}$$

$$iQ = ha\left[\frac{2mw}{\hbar^2} - G_z^2 + \frac{2mw}{\hbar^2} - F_z^2\right] \qquad \text{(A1)}$$

letting $U = \cos^{-1}(z/ha)$

$$(K_{F_z}|V_H|K_{G_z}) = \frac{2B\delta_{H_y,0}hawe^{-Q}}{\sqrt{c_G c_F}}\,e^{i[G_z - F_z^*]ha} \qquad \text{(A2)}$$

where F_z^* = the complex conjugate of F_z.

$$\text{with } B = \int_0^{\pi} du \, \frac{\sin u \sin ju \, e^{iQ \cos u}}{ju} \tag{A3}$$

one can easily show

$$e^{iQ \cos u} = \sum_{n=0}^{\infty} b_n \cos nu \tag{A4}$$

where $b_n = 2(i)^n J_n[Q]$

$b_o = J_o[Q]$

substituting into the integral

$$B = \sum_{n=0}^{\infty} b_n \sigma[j,n] \tag{A5}$$

with

$$\sigma[j,n] = \int_0^{\pi} du \, \frac{\sin u \sin ju \cos nu}{ju} \tag{A6}$$

Direct evaluation gives

$$\sigma[j,n] = \frac{1}{4j} \text{Cin}[|n - j + 1|\pi] + \text{Cin}[|j + 1 - n|\pi] - \text{Cin}[|n + j - 1|\pi]$$

$j \neq 0$

$$= \frac{\pi}{2}(\delta_{|n|,1} + \delta_{n,o}) \qquad j = 0$$

in the limit $w \to \infty$

$$Q \to 2iha\sqrt{\frac{2mw}{\hbar^2}} + O\left(\frac{1}{\sqrt{w}}\right)$$

since $|Q| \to \infty$ (from Abramowitz 9.2.1, 17)

$$J_n(Q) = \frac{2}{\pi Q} \cos(Q - \tfrac{1}{2}n\pi - \tfrac{1}{4}\pi) + O|Q^{-1}|$$

and since

$$\cos x = \frac{e^{ix} + e^{-ix}}{2}$$

$$J_n(Q) = \sqrt{\frac{-i}{2\pi Q}} \quad (-i)^n e^{iQ} + O(Q^{-\frac{3}{2}}) \qquad \text{(A7)}$$

Combining equations A2-A7 yields

$$(K_{F_z}|V_H|K_{G_z}) = e^{i[G_z - F_z^*]ha} \frac{\delta_{H_y,0} haw}{\sqrt{c_g c_f}} \sqrt{\frac{1}{4\pi ha\sqrt{\frac{2mw}{\hbar^2}}}} (\sigma[j,0] + 2\sum_n \sigma[j,n]) + O(W^{\frac{1}{4}})$$

so that

$$(K_{F_z}|V_H|K_{G_z}) \propto w^{\frac{3}{4}}$$

which approaches ∞ for large w.

An approximation valid for smaller values of w can be obtained as follows:

Define ξ by

$$\xi \equiv iQ$$

$$J_n[Q] = J_n[-i\xi] = (-i)^n I_n[\xi]$$

Notice that as $w \to \infty$

$$\xi \to 2\sqrt{\frac{2mw}{\hbar^2}} \left(1 + \frac{\left(F_z^2 - G_z^2\right)\hbar^2}{8mw} + O(W^{-2})\right)$$

which is large, real and positive.

For large ξ, Abromowitz (9.7.1) [17] gives

$$I_n[\xi] = \frac{e^{\xi}}{\sqrt{2\pi\xi}}\left(1 - \frac{(4n^2 - 1^2)}{8\xi} + \frac{(4n^2 - 1^2)(4n^2 - 3^2)}{2!(8\xi)^2} + \ldots\right) \qquad \text{(A8)}$$

Combining A2-6 and A8 yields

$$(K_{F_z}|V_H|K_{G_z}) = \frac{e^{i[G_z - F_z^*]ha}}{\sqrt{c_g c_f}} \delta_{H_y,0} w \sqrt{\frac{1}{ha\sqrt{\frac{2mw}{h^2}}}}$$

$$\times \left[1 - \frac{\left(F_z^2 - G_z^2\right)\hbar^2}{16mw} + O(w^{-2})\right] \left\{ \sigma(j,0) \left[1 + \frac{1}{8ha\sqrt{\frac{2mw}{\hbar^2}}} - \frac{9\hbar^2}{256mwh^2a^2} + \emptyset(w^{-\frac{3}{2}}) \right] + 2 \sum_{n=1}^{\infty} \sigma(j,n) \left[1 - \frac{\left(4n^2 - 1^2\right)}{8ha\sqrt{\frac{2mw}{\hbar^2}}} + \frac{[4n^2 - 1^2][4n^2 - 3^2]\hbar^2}{256mw\, h^2a^2} + O(w^{\frac{3}{2}}) \right] \right\} \tag{A9}$$

Combining terms

$$(K_{F_z}|V_H|K_{G_z}) = \left\{ \frac{\delta_{H_y,0}\, e^{i(G_z - F_z^{\dagger})ha}}{\sqrt{c_g c_f}} \sqrt{\frac{1}{ha\pi\sqrt{\frac{2m}{\hbar^2}}}} \left[\sigma(j,0) + 2\sum_n \sigma(j,n)\right] \right\} (w^{\frac{3}{4}})$$

$$+ \left\{ \frac{\delta_{H_y,0}\, e^{i(G_z - F_z^{*})ha}}{\sqrt{c_g c_f}} \sqrt{\frac{1}{\pi ha\sqrt{\frac{2m}{\hbar^2}}}} \frac{1}{8ha\sqrt{\frac{2m}{\hbar^2}}} \left[\sigma(j,o) + 2\sum_n \sigma(j,n)[4n^2 - 1]\right] \right\} w^{\frac{1}{4}}$$

$$+ O(w^{-\frac{1}{4}}) \tag{A10}$$

Therefore the A matrices are either (for large w)

1. proportional to $w^{\frac{3}{4}}$
2. proportional to $w^{\frac{1}{4}}$

} approach infinity

3. approach zero

The CCGM method predicts that there will be only specular scattering whenever the A matrix elements are infinte or zero.

APPENDIX B

Semiclassical calculations for scattering at normal incidence from a sinusoidal hardwall, assuming only one classical scattering event.

Starting with the surface contour

$$D(x) = ha\cos(2\pi\frac{x}{a}) \tag{B1}$$

One can show that in the classical single scattering limit,

$$\theta(x^*) = 2\tan^{-1}[2\pi h\sin(\frac{2\pi x^*}{a})] + \theta_I \tag{B2}$$

For normal incidence ($\theta_I = 0$)

$\hat{x} = x^*$.

Defining a quantum number function by:

$$\ell = \frac{\Delta k_x a}{2\pi} \tag{B3}$$

one can show

$$\ell(\hat{x}) = \frac{2kah\sin\frac{2\pi\hat{x}}{a}}{1 + (2\pi h)^2\sin\frac{2\pi\hat{x}}{a}} \tag{B4}$$

the change in phase due to the collision $\phi(x)$, defined as

$$\phi(\hat{x}) \equiv -\int dt(zp_z + xp_x) \tag{B5}$$

is given by

$$\phi(\hat{x})/\hbar = \frac{-2\pi\ell\hat{x}}{a} - hka\cos(\frac{2\pi x}{a})\left(1 + \sqrt{1 - \left(\frac{2\ell\pi}{ka}\right)^2}\right) \tag{B6}$$

For any ℓ, there are two trajectories, and therefore two values of $\hat{x}$, that satisfy equation B4, they are

$$\hat{x}_1 = \frac{a}{2\pi}\sin^{-1}\left[\left(\frac{ka}{2n\pi}\right)\frac{1}{2\pi h}\left(1 - \sqrt{1 - \left(\frac{2\ell\pi}{ka}\right)^2}\right)\right] \tag{B7}$$

$$\hat{x}_2 = a/2 - \hat{x}_1$$

In the primitive semiclassical approximation the intensity, I_ℓ, of the ℓth order diffraction peak is*

---

*the factor $\cos\theta_\ell$ comes because the P_ℓ's are normalized via equation 9.

$$P_\ell = a\left(\sum_\rho \left[\frac{\partial \ell}{\partial \bar{x}_\rho}\right]^{-\frac{1}{2}} e^{i\Phi_\rho}\right)^2 (\cos\ \theta_\ell)$$

where ρ is an index of paths scattering in the direction defined by the index ℓ.

which becomes

$$P_\ell = P_C^\ell\ 2\ \sin^2\left(\frac{\pi}{4} + \frac{\Delta\Phi_\ell}{2\hbar}\right)\cos\ \theta_\ell$$

with

$$P_{C\ell}^\ell = \frac{ka}{(2n\pi)^2}\left(1 - \sqrt{1 - \left(\frac{2\pi\ell}{ka}\right)^2}\sqrt{1 - \left(\frac{2\pi\ell}{ka}\right)^2}\right.$$

$$\left.\sqrt{(2\pi h)^2 - \left(\frac{ka}{2\pi\ell}\right)^2\left(1 - \sqrt{1 - \left(\frac{2\pi\ell}{ka}\right)^2}\right)}\right)$$

To be consistant with our previous work (13), Bessel function uniformization will be used.

Following the prescription of Marcus, et al., ζ will be determined by

$$\sqrt{\zeta^2 - \ell^2} - \ell\cos^{-1}\left(\frac{\ell}{\zeta}\right) = \frac{\Delta\phi}{2\hbar} \qquad \text{(B8)}$$

one can verify that

$$\zeta = hka(1 + \cos\ \theta_\ell) \qquad \text{(B9)}$$

P_ℓ becomes

$$P_\ell = P_{C\ell}\frac{\pi}{2}\ (\zeta^2 - \ell^2)^{\frac{1}{2}}\ J_\ell^2(\zeta)\cos\theta_\ell \qquad \text{(B10)}$$

Combining equations B9 and B10 yields the result quoted in the main text

$$P_\ell = J_\ell[hka(1 + \cos\ \theta_\ell)]^2 \qquad \text{(B10)}$$

APPENDIX C

In Appendix B we assumed that the trajectory only undergoes one classical scattering event. In this section, the validity of that approximation will be examined.

From the previous section, we know that a particle incident on the surface at a point x* will scatter at an angle θ.

$$\theta = 2 \tan^{-1}\left[2\pi h \sin \frac{2\pi x^*}{a}\right] + \theta_I \tag{C1}$$

The trajectory of the particle is given by

$$z = D(x^*) + \frac{\hbar k}{m} t \cos \theta \tag{C2}$$

$$x = x^* + \frac{\hbar k}{m} t \sin \theta$$

where k is the incident particles's k vector, m is their mass and t is time measured from the impact.

Defining a function Ω by

$$\Omega(x^*,t) = \frac{z - D(x)}{\frac{\hbar k t}{m}} \tag{C3}$$

one can observe that if Ω is positive for all real $t \geq 0$, the trajectory will only scatter once.

A convenient way to tell if multiple scattering is important in a given range of x* is to examine the function

$$\omega = \underset{t,x^*}{\text{Min}} \left[\Omega(x^*,t)\right] \tag{C4}$$

If ω is positive, there will not be any classical multiple scattering. If ω is negative, classical multiple scattering will occur.

The necessary range of x* still has to be determined. In principle, a semiclassical calculation must include all values of x*, both real and complex. Physically, the trajectories corrdsponding to real values of x* are the classically allowed

trajectories, while the trajectories corresponding to complex values of x* are the classically unallowed, or tunneling, trajectories. The classically unallowed trajectories only have a significant effect on the scattering intensity oustide of the classical rainbow angles. Most of the scattering occurs between the classical rainbow angles. For the moment, we will restrict our attention to those trajectories that scatter between these angles. For this purpose, x* can be assumed to be real. ω can be calculated using a search procedure.

A plot of ω as a function of h at constant θ_I can then be constructed. At any given θ_I, the value of h that satisfies $\omega = 0$ can then be calculated. It will be denoted by h*. If $h < h^*$, classical multiple scattering should be unimportant. At higher roughnesses, classical multiple scattering occurs. Table 1 gives values of h* as a function of θ_I, determined via this procedure.

If we assume that the range of x*/a's that will minimize Ω for all θ is known, then h* can be bounded. One can show

$$h^* = h_o \frac{(1-|\sin \theta_I|)}{\cos \theta_I} \qquad \text{(C5)}$$

where h_o = the critical value at h, calculated at normal incidence, assuming that the given value of x*/a is correct.

For normal incidence, x*/a = .2958 so that h_o = .130. At grazing incidence, x*/a < .2651, and h_o = .143. (It is slightly higher in this case because x*/a is away from the minimum for normal incidence.) Table 1 also gives values of h* calculated for h_o = .130 and .143. One can see that they bound the numerical calculations. This is the basis of equation 52 in the main text.

This, of course, has only considered scattering between the classical rainbow angles, where x* can be assumed to be real. Beyond these angles, complex x* must be included. The definition of classical multiple scattering in the classically unallowed region is unclear, and so we have not defined any criterion for it. We note that if a trajectory scatters at an angle θ, so that

$$\theta \leq \tan^{-1}(1/4h) \tag{C6}$$

it cannot multiply scatter. This is the second criterion in the main text.

APPENDIX D--AN ALTERNATE DERIVATION OF EQUATION 28

Starting with the Lippmann-Schwinger equation

$$\psi = \Phi_I + \int_{-\infty}^{\infty} dx' \int_{-\infty}^{\infty} dz' \; G_o^+(x,z;x',z')V(x',z')\psi(x',z') \qquad (D1)$$

and substituting for $V\psi$ from the Schroedinger equation yields

$$\psi = \Phi_I + \int_{-\infty}^{\infty} dx' \int_{-\infty}^{\infty} dz' \; G_o^+(x,z;x',z')(\nabla^2\psi + E\psi) \qquad (D2)$$

The arguments in our previous paper (i.e., that $V\psi=0$ except infinitesimally near the surface) show that the only contribution to the integral comes at the surface so that the limits on the integral can be changed to

$$\psi = \Phi_I + \int_{-\infty}^{\infty} dx' \int_{D(x)-\Delta}^{D(x)+\Delta} dz' \; G_o^+(x,z;x',z')(\nabla^2\psi + E\psi) \qquad (D3)$$

where Δ is a positive infinitesimal.

The $E\psi$ term vanishes since $\psi=0$ in this region. Applying Greenes' first theorem to the $\nabla^2\psi$ term yields

$$d\,\psi = \Phi_I + \int_{-\infty}^{\infty} \left.\frac{\partial\psi}{\partial\underset{\sim}{n}}\right|_{z=D(x)+\Delta} ds + \int_{-\infty}^{\infty} \left.\frac{\partial\psi}{\partial\underset{\sim}{n}}\right|_{z=D(x)-\Delta} ds + \int_{-\infty}^{\infty} dx' \int_{D(x)-\Delta}^{D(x)+\Delta} dz' \; \nabla G_o^+ \nabla\psi \qquad (D4)$$

The second integral vanishes since $\frac{\partial\psi}{\partial\underset{\sim}{n}}$ is zero everywhere below the surface. The third integral vanishes as $\Delta \to 0^+$ since it is the integral of a finite function over an infinitesimal area. Q.E.D.

References

1. For recent reviews see: W.H. Weinberg, Adv. Colloid Interface Sci. 4, 301 (1975); A.G. Stoll, R.E. White, R.I. Masel and R.P. Merrill, J. Vac. Sci. Tech. 12, 192 (1975).
2. G. Wolken: J. Chem. Phys. 58, 3047 (1973), 59, 1159 (1973); Chem. Phys. Lett., 21, 373 (1973); J. Chem. Phys. 61, 456 (1974).
3. A. Tsuchida, Surf. Sci. 14, 375 (1969).
4. J.L. Beeby: J. Phys. C 4, L359 (1970), 5, 34, 38 (1972), 5, 3457 (1972), 6, 1229 (1973); Jpn. J. App. Phys. Supp. 2 Pt. 2, 537 (1974).
5. R.I. Masel, R.P. Merrill and W.H. Miller, submitted to J. Phys. C.
6. A.C. Levi, U. Garibaldi, R. Spadachini and G.E. Tommei: Jpn. J. App. Phys. Supp. 2 Pt. 2, 549 (1974); Surf. Sci., to be published.
7. M.V. Berry, J. Phys. A 8, 566 (1975).
8. F.O. Goodman, N. Cabrera, V. Celli and J.B. Mason, Surf. Sci. 19, 67 (1970); F.O. Goodman, Surf. Sci. 19, 93 (1970), 46, 118 (1974); F.O. Goodman, J. Chem. Phys. 58, 5530 (1973); F.O. Goodman and W.K. Tan, J. Chem. Phys. 59, 1805 (1973).
9. J.D. Doll: J. Chem. Phys. 61, 954 (1974); Chem. Phys. 3, 257 (1974).
10. R.I. Masel, R.P. Merrill and W.H. Miller, J. Chem. Phys. 64, 45 (1976).
11. J.M. Bowman and C.J. Ray, J. Chem. Phys. 63, 5231 (1975).
12. P. Beckman and A. Spizzichino, The Scattering of Electromagnetic Waves from Rough Surfaces, Pergamon Press, 1963.
13. R.I. Masel, R.P. Merrill and W.H. Miller, Phys. Rev. B 12, 5545 (1976).

14. W.H. Miller: Adv. Chem. Phys. 25, 69 (1974); J. Chem. Phys. 53, 1949 (1970).

15. R.A. Marcus: Chem. Phys. Lett. 7, 525 (1970); J. Chem. Phys. 59, 5135 (1973).

16. J.A. DeSanto, J. Acoust. Soc. AM 57, 1195 (1975).

17. M. Abramowitz and I. Stegun, Handbook of Mathematical Functions, Dover, NY (1970).

18. H. Rabitz, J. Chem. Phys. 55, 400 (1971). see especially Figure 7.

19. R. Petit and M. Cadilhac, Comptes Rendes Acad. Sci. Ser. B202, 469 (1966).

Figure Captions

Figure 1: The scattering intensity as a function of angle for the "exact" calculations with: a) h=0.02, K_a=30; b) h=0.02, K_a=40; c) h=0.02, K_a=60; d) h=0.04, K_a=40; e) h=0.10, K_a= 20.

Figure 2: Typical trajectories from hard (2a) and soft (2b) surface potentials.

Figure 3: The intensity of the specular beam at normal incidence with h=0.02 as a function of k-vector, calculated by the "exact" (——), uniform semiclassical (x), and renormalized semiclassical (◇) methods.

Figure 4: The first order beam for the same conditions as in Fig. 3.

Figure 5: The second order beam for the same conditions as in Fig. 3.

Figure 6: Intensity of the specular beam at normal incidence with h=0.10, calculated by the "exact" (—), renormalized uniform semiclassical (x), and uniform semiclassical (O and ◇) methods. Two symbols are used for the uniform semiclassical to emphasize the change in scale.

Figure 7: Quasiclassical calculations for the same conditions as in Fig. 6.

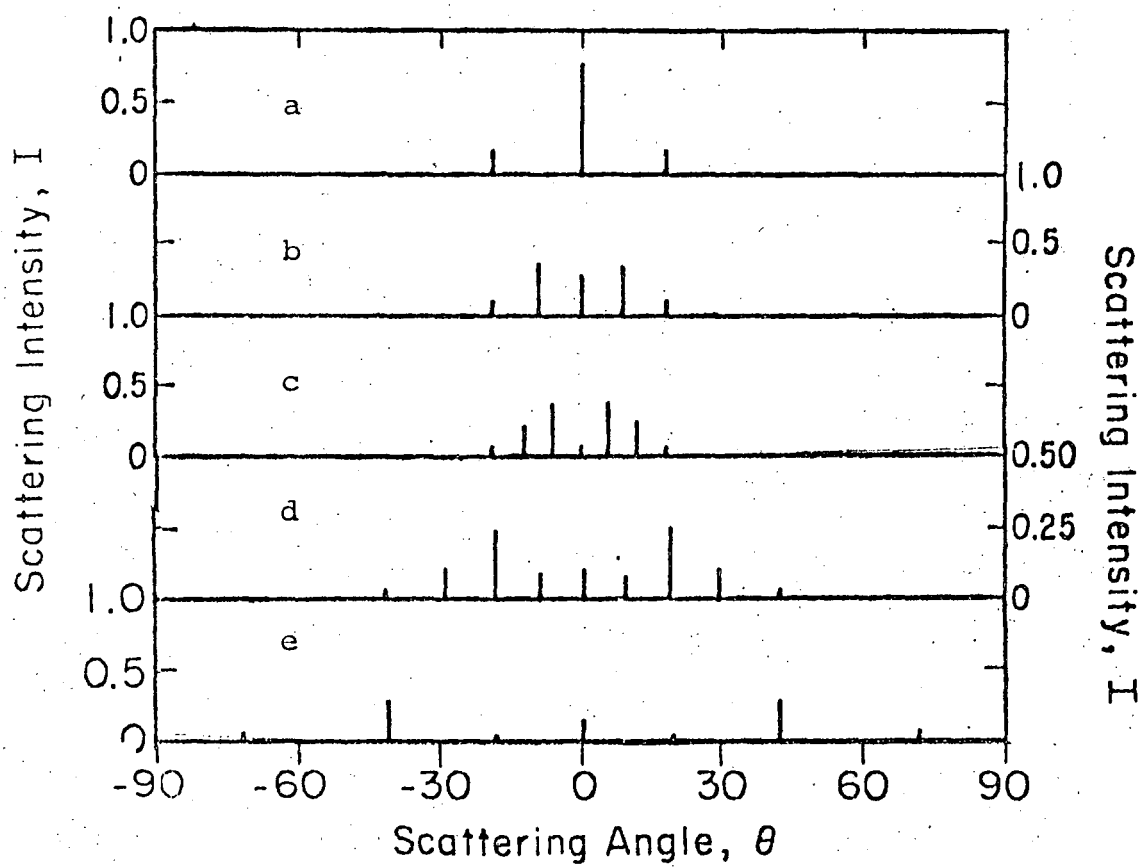
Scattering Intensity, I
1.0
0.5
0
a
b
c
d
e
1.0
0.5
0
1.0
0.5
0
1.0
0.5
0
1.0
0.5
0
0.50
0.25
0
-90
-60
-30
0
30
60
90
Scattering Angle, θ
Scattering Intensity, I

Figure 1

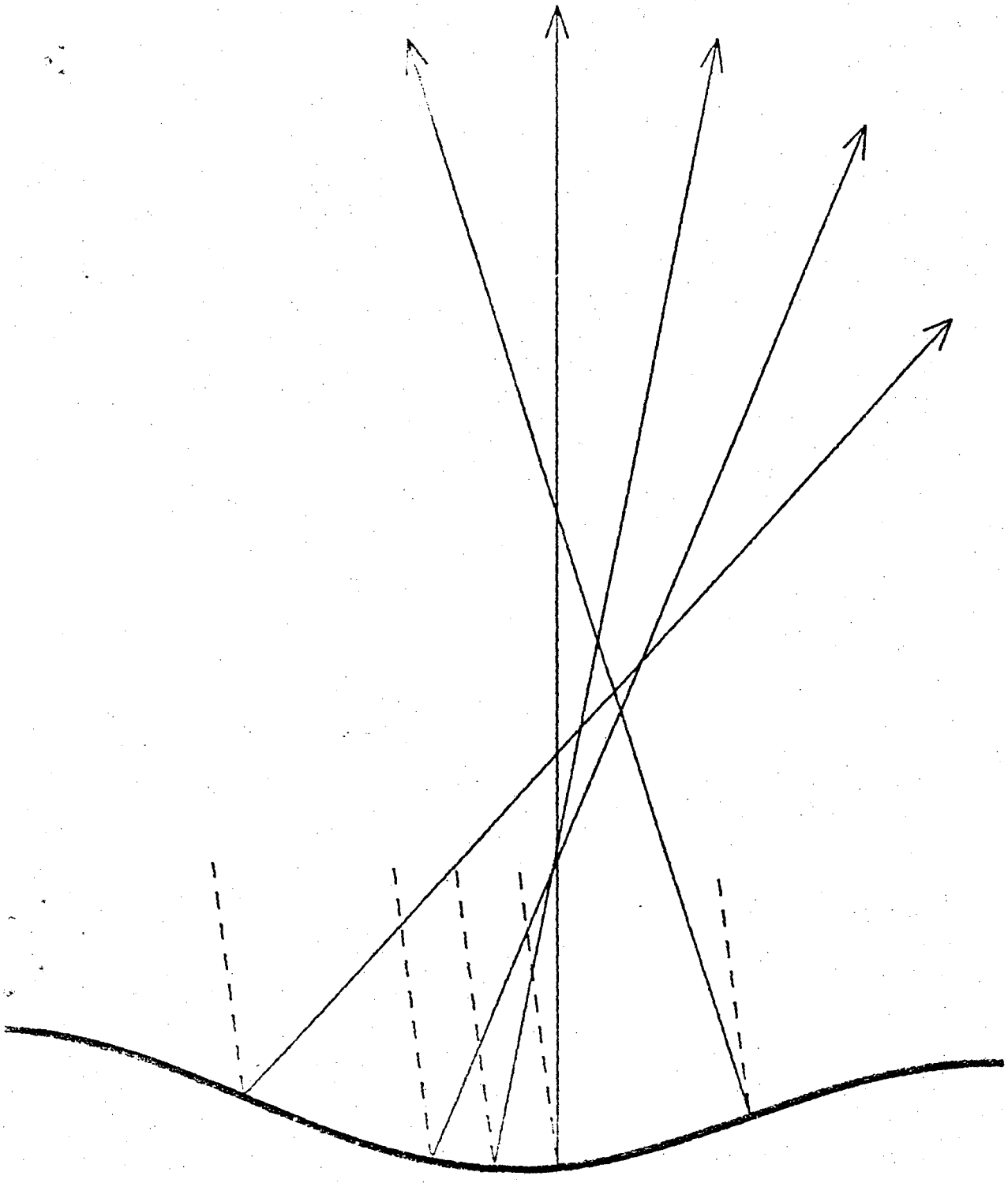

Figure 2a

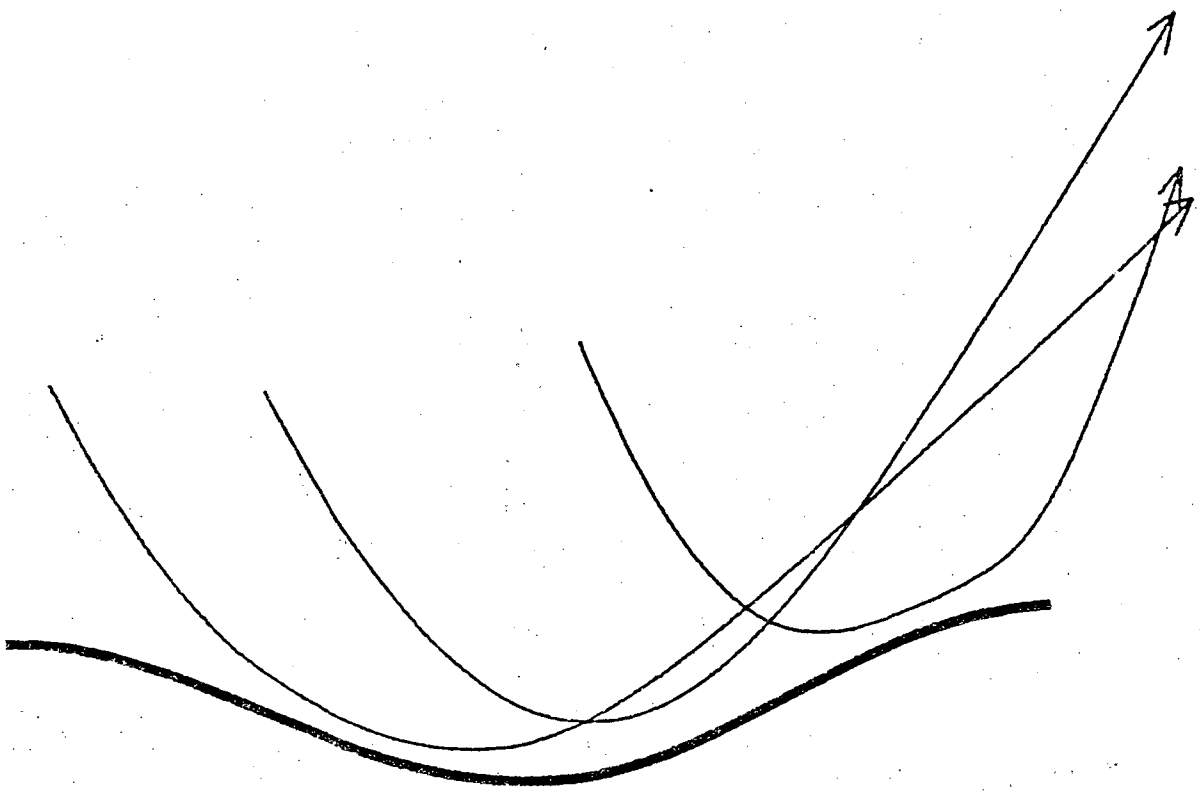

Figure 2b

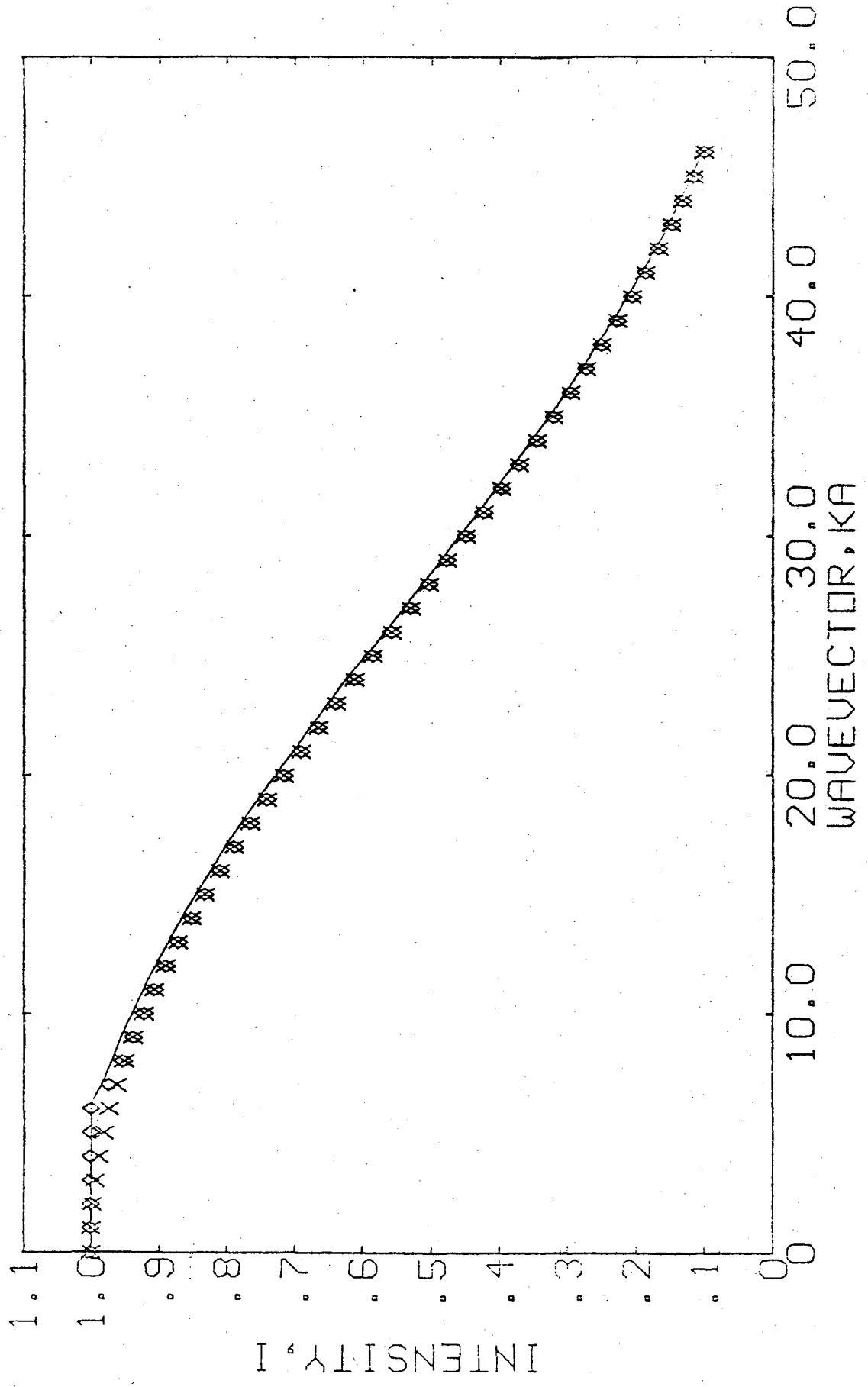
INTENSITY, I
1.1
1.0
.9
.8
.7
.6
.5
.4
.3
.2
.1
0
0
10.0
20.0
30.0
40.0
50.0
WAVEVECTOR, KA

Figure 3

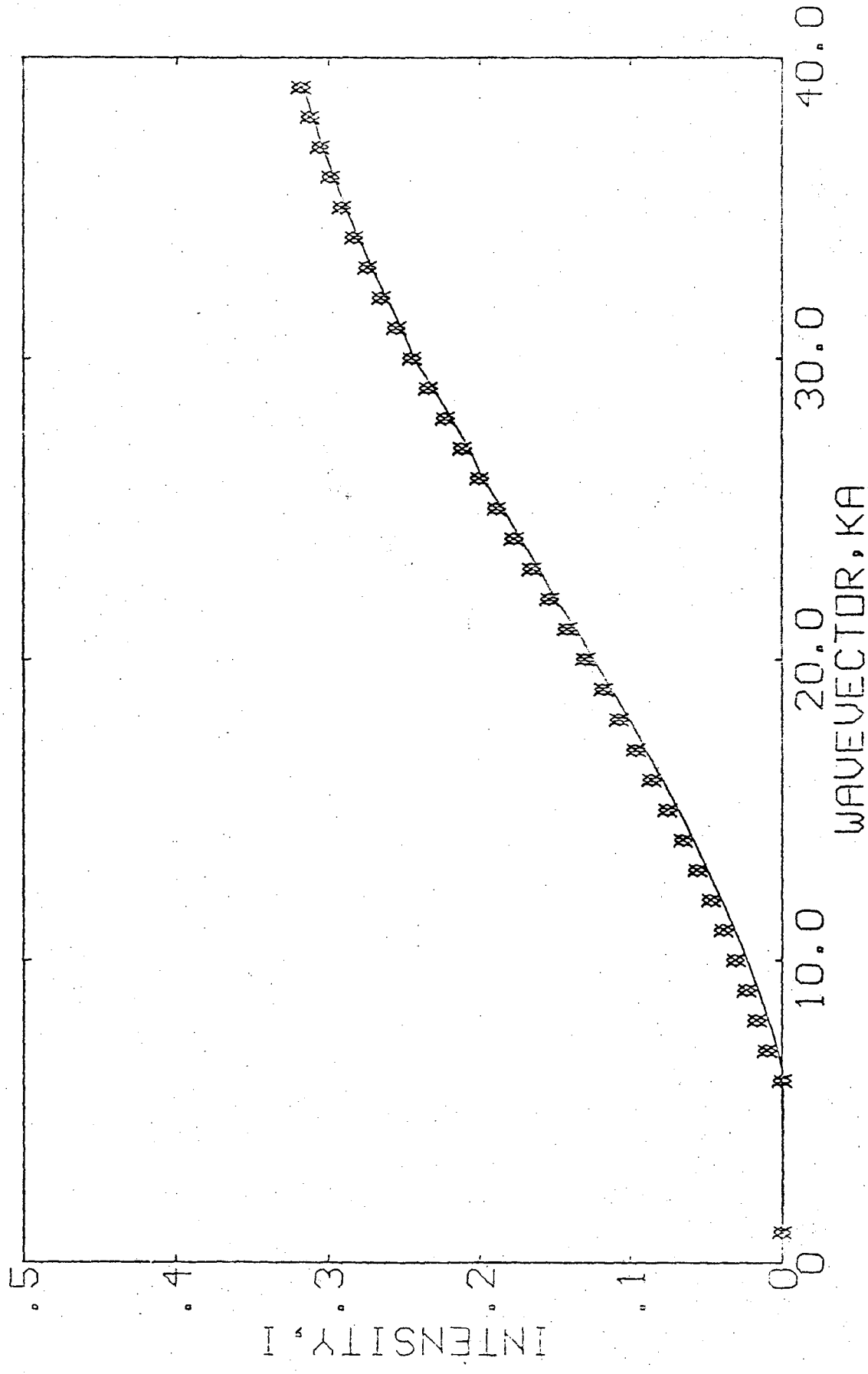

Figure 4

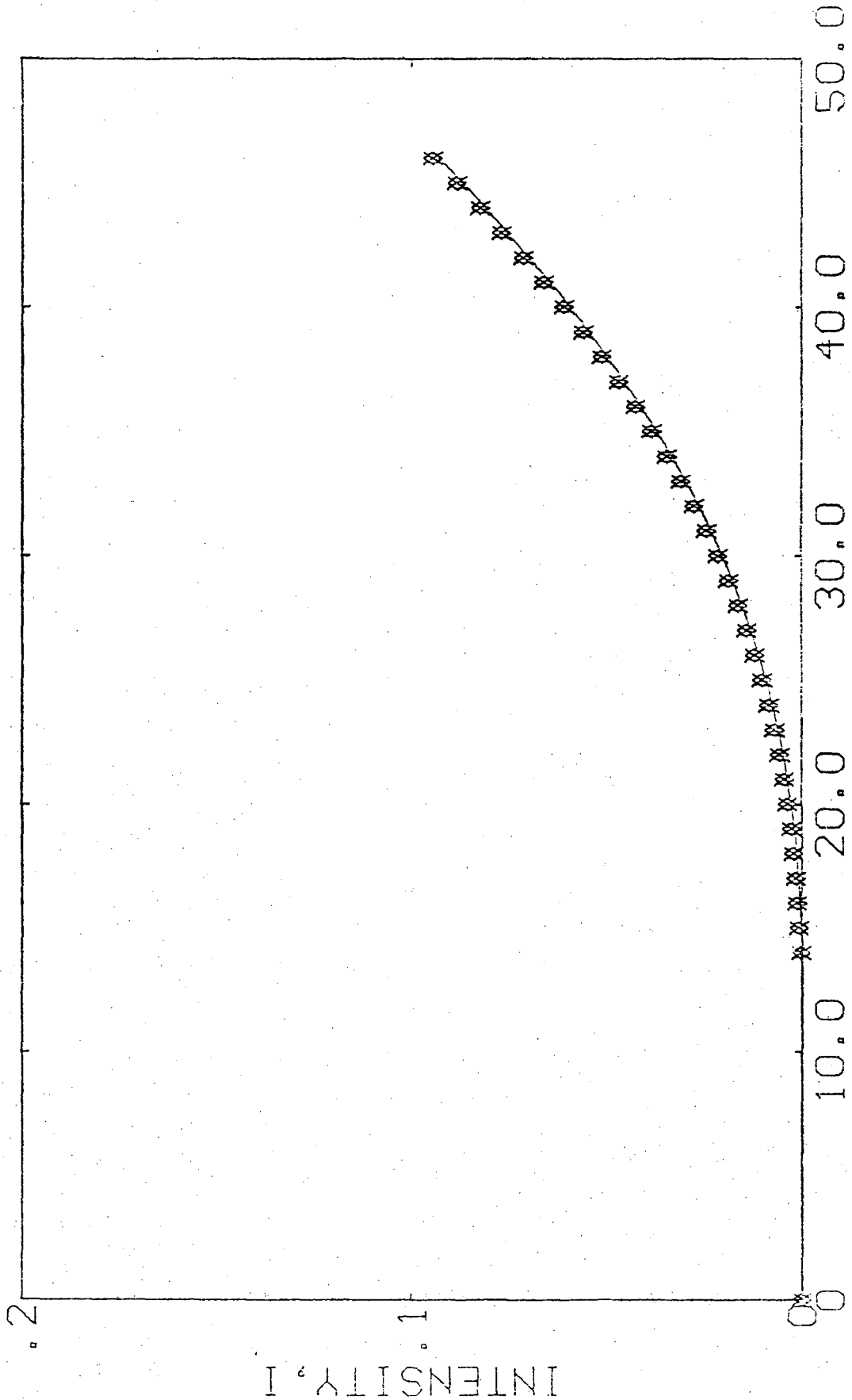

Figure 5

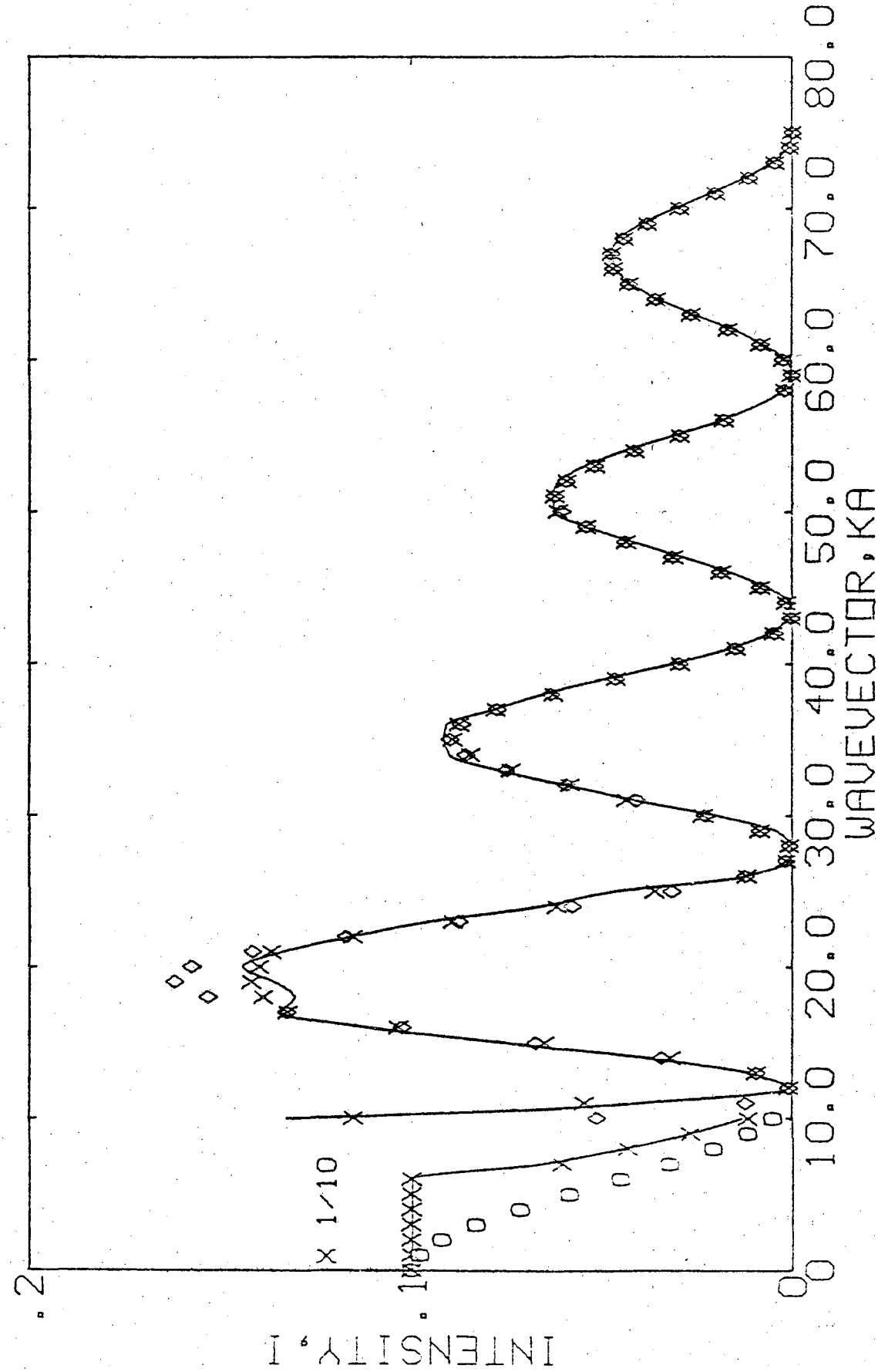
INTENSITY, I
.2
.1
0
0
10.0
20.0
30.0
40.0
50.0
60.0
70.0
80.0
WAVEVECTOR, KA
x 1/10

Figure 6

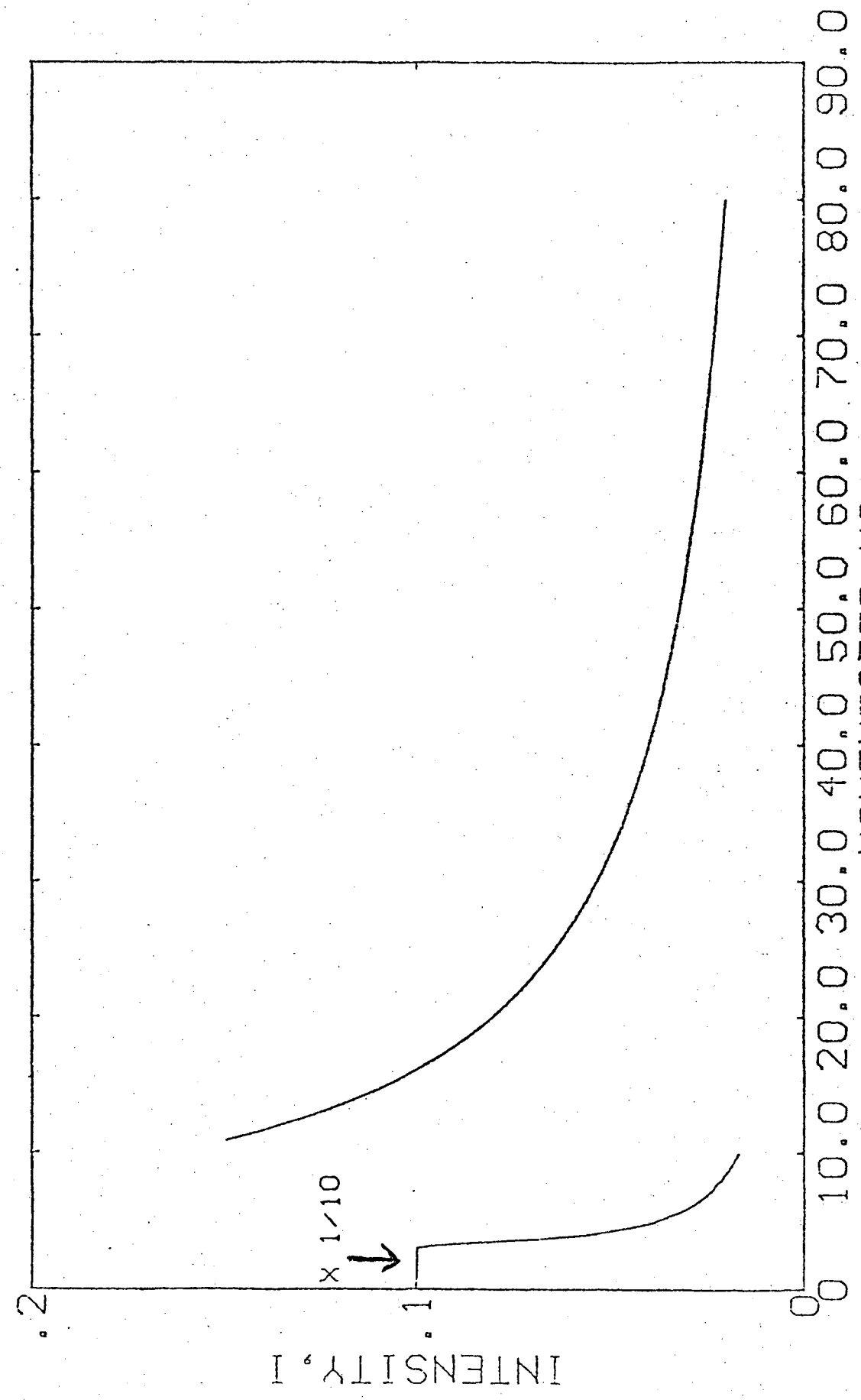
INTENSITY, I
.2
.1
0
x 1/10
0 10.0 20.0 30.0 40.0 50.0 60.0 70.0 80.0 90.0
WAVEVECTOR, KA

Figure 7

TECHNICAL INFORMATION DIVISION
LAWRENCE BERKELEY LABORATORY
UNIVERSITY OF CALIFORNIA
BERKELEY, CALIFORNIA 94720